



Article

Biodegradable Polymers Grafted onto Multifunctional Mesoporous Silica Nanoparticles for Gene Delivery

Egídio Paulo Francisco Nhavene ¹, Gracielle Ferreira Andrade ¹ ,
Jerusa Araujo Quintão Arantes Faria ², Dawidson Assis Gomes ³ and
Edésia Martins Barros de Sousa ^{1,*} 

¹ Centro de Desenvolvimento da Tecnologia Nuclear—CDTN, Avenida Presidente Antônio Carlos, 6.627 Campus UFMG, Belo Horizonte, 31270-901 MG, Brazil; egidionhavene@yahoo.com.br (E.P.F.N.); graciellefandrade@yahoo.com.br (G.F.A.)

² Departamento de Ciências Fisiológicas—ICB, UFAM, Manaus, 69080-900 AM, Brazil; jerusaquintao@gmail.com

³ Departamento de Bioquímica e Imunologia—ICB, UFMG, Belo Horizonte, 31270-901 MG, Brazil; dawidson@icb.ufmg.br

* Correspondence: sousaem@cdtn.br; Tel.: +55-31-3069-3223

Received: 6 April 2018; Accepted: 22 May 2018; Published: 28 May 2018



Abstract: Biodegradable polymer possesses significant potential for applications in different fields, since flexibility gives rise to materials with great physical and mechanical property diversity. The poly-caprolactone (PCL) and chitosan derivatives (CS) have the ability to form scaffolds, which adhere to the surface of mesoporous silica nanoparticles (MSNs) and its porous networks. The novel characteristics of the developed PCL/MSNs and CS/MSNs, such as very low in vivo degradation rate, ordered pore network, uniform and tunable size and shape of the particles, high pore volume and surface area, non-toxicity, and biocompatibility, among others, are responsible for its favorable gene delivery device and makes this conjugation a very good biomaterial for this application. In the present study, we investigated the synthesis of silica nanoparticles MCM-41 covalently grafted with PCL and CS and their use as a potential small interfering RNA (siRNA) carrier. The physical–chemical and morphological characterizations, as well as the applicability of functionalized MSNs as platforms for gene delivery, were assessed. Our results confirmed that MSNs that were successfully functionalized with PCL and CS kept their typical morphology and pore arrangement. Furthermore, their surface modification was successfully held. In vitro biocompatibility and cytotoxicity assays suggest the ability of MSNs to support passive uptake and indicated the potential of this material as a gene delivery system for cervical cancer cells (HeLa).

Keywords: MCM-41; poly-caprolactone; chitosan; surface functionalization; bioapplication

1. Introduction

Among the nanostructured materials, the mesoporous silica nanoparticles (MSNs) are a new generation of inorganic platforms for bioapplications. Due their physico-chemical properties such as low toxicity and high drug loading capacity, they are used in controlled and targeted drug delivery, and safe and efficient gene delivery systems [1,2].

There are several types of MSNs; one of them is the Mobil Composition of Matter No. 41 (MCM-41) developed in 1996 by researchers at Mobil Oil Corporation [3]. The MCM-41 nanoparticles possess unique physico-chemical properties, an ordered pore network structure with hundreds of empty channels, tunable pore size (2 to 10 nm diameter of mesopores), high pore volume ($\sim 1 \text{ cm}^3 \cdot \text{g}^{-1}$),

and high surface area ($1200 \text{ m}^2 \cdot \text{g}^{-1}$) [2]. Together, these properties allow for the easy functionalization of the silanol containing groups on a surface that is able to absorb or encapsulate relatively large amounts of bioactive molecules [4].

New approaches show the functionalization of the silanols groups with cross-linked biodegradable polymers has been highlighted as a promising way of obtaining versatile and multifunctional MSNs.

The MSNs can be linked to metals ions to enhance the biological applications and design the copper metal with aminotriazole functionalizing MSNs that inhibits antioxidant defenses and catalyzes the activation of lethal reactive oxygen species (ROS) using the framework of copper ions to kill cancer [5]. Cu metal was also impregnated in the framework of MSNs for enhancing the doxorubicin (Dox) loading through coordination interactions, which facilitates the release precisely in the tumoral acidic environment [6].

Furthermore, the biodegradable cationic polymer-modified MSNs nanoparticles have attracted great interest because of the high density of cationic charges on the surface that could be used as nonviral vectors [7] and drug carriers [8] and can serve as a biocompatible and effective breast cancer-targeting and theranostic agent [9–12].

Hung et al. [9] show the amino-functionalized MSNs conjugated with glutaraldehyde stabilize enzymes in nanochannels through the formation of covalent imine bonds in prodrug cancer therapy. Another research group reported MSNs functionalized with the monoclonal antibody Herceptin are effective for breast cancer imaging, diagnosis, and treatment [10].

Liong et al. [11] reported the preferential uptake of folic acid-conjugated MSNs into pancreatic cancer cell lines was able to release their drug payload into the cytosol, reducing cancer cell survival by 60%. Meng et al. [12] have demonstrated that MSNs can co-deliver anti-cancer drug and siRNA, thus increasing anti-cancer drug efficacy, mitigating drug resistance via the use of siRNA, and reducing systemic drug release prior to MSNs' delivery to cancer cells.

The biodegradable cationic polymers are efficient at condensing negatively charged DNA into MSNs nanoparticles via a strong electrostatic interaction and low immunogenicity [7].

Polycaprolactone (PCL), which is a biodegradable polyester that is easy to synthesize, manipulate, and blend, besides being non-toxic, has been widely used, with amino groups being effective in the drug-controlled and gene-release applications [13]. PCL easily adheres to surfaces of MSNs by mixing with a wide range of inorganic and organic platforms, enhancing physical–chemical properties and advantageous characteristics such as biodegradability, biocompatibility, and anchoring capacity for bioapplications [14].

Chitosan (CS) is another biodegradable cationic polymer, which is a structural polysaccharide component naturally occurring in crustacean and insect shells, derived from the partial deacetylation alkaline of chitin, which consists of repeating units of glucosamine and *N*-acetylglucosamine [15].

Several studies have shown that it is one of the most prominent, naturally derived nonviral vectors for gene transfer due to its protonatable amine groups on structure while bearing advantageous characteristics such as biodegradability and biocompatibility [16].

In order to improve the gene delivery efficiency, different strategies for the structural modification of the biodegradable cationic polymers with MCM-41 nanoparticles have been studied to promote cellular uptake. There are high expectations that gene therapy can cure some diseases caused by genetic disorders, and for this, vehicles for efficient gene delivery are required for release of the payload at target intracellular locations using biodegradable cationic polymers enveloped by MCM-41 nanoparticles. Both the PCL and CS have the ability to form scaffolds, which adhere onto the surface and porous networks of MCM-41.

In this work, we used PCL and CS covalently attached by crosslink molecules to the surface of porous MCM-41 nanoparticles to act as an anchor for siRNA delivery in HeLa cells. The preparation method and main characterizations of the obtained MCM-41 are investigated. The *in vitro* test of biocompatibility and cytotoxicity suggests the ability of MCM-41 to support passive cellular uptake and consequently indicated its application as potential nanocarrier biomaterials. The results showed

that one of the great expectations offered by nanobiotechnology, which through gene therapy can cure some diseases caused by genetic disorders, do not present many treatment alternatives.

2. Materials and Methods

2.1. Materials

(3-aminopropyl)triethoxysilane (APTES), acetone, acetic acid glacial ($\text{CH}_3\text{CO}_2\text{H}$), chitosan (CS), ethyl alcohol pure (EtOH), (3-glycidoxypropyl)trimethoxysilane (GPTMS), sodium hydroxide (NaOH), chloride acid (HCl), succinic anhydride (Suc) ($\text{C}_4\text{H}_4\text{O}_3$), tetraethylorthosilicate (TEOS), texadecyltrimethylammonium bromide (CTAB), and poly- ϵ -caprolactone (PCL) were purchased from Sigma-Aldrich (São Paulo, Brazil). The Fibroblast and HeLa cells were treated with Dulbecco's modified eagles' medium-high glucose (DMEM), penicillin, streptomycin, and amphotericin (PSA), and fetal bovine serum, which were all purchased from Sigma-Aldrich, as well as MTT (3-(4,5-dimethylthiazolyl-2)-2,5-diphenyltetrazolium bromide). The siRNAs were purchased from Eurogentec, Seraing, Belgium).

2.2. Methods

2.2.1. Synthesis of Mesoporous Silica Nanoparticles—MCM-41

MCM-41 silica was prepared in accordance with a published procedure [17] using commercial CTAB as a template agent in basic conditions. CTAB (2.74 mmol) and NaOH (7.00 mmol) were dissolved in 480 mL of Milli-Q[®] water. The temperature of the mixture was adjusted to 75 °C, and after that, 22.4 mmol of TEOS was added dropwise to the surfactant solution under vigorous stirring. The mixture was reacted for 2 h to give rise to a white precipitate, which was filtered, washed with Milli-Q[®] water and ethanol, and dried at 37 °C for 24 h. The surfactant was removed by calcination, which was carried out by increasing the temperature to 550 °C under nitrogen flow for 2 h followed by 3 h in air.

2.2.2. Functionalization of Mesoporous Silica MCM-41 with (3-Glycidoxypropyl)trimethoxysilane (GPTMS)

300 mg of MCM-41 was dispersed in 20 mL of EtOH by ultrasonication for 30 min, and the pH value was adjusted to 6–7, under magnetic stirring. Subsequently, 1 mL of GPTMS was dropwise added into MCM-41 in EtOH dispersion with magnetic stirring. The mixture was kept under constant magnetic stirring at 50 °C for 5 h. At the end, the suspension was filtered and washed thoroughly with Milli-Q[®] water and acetone followed by drying at 37 °C for 2 days. This sample was named MCM-41 + GPTMS, and it will be used as a bridge to link MCM-41 and CS.

2.2.3. Functionalization of Mesoporous Silica MCM-41 with GPTMS and Chitosan

In the next functionalization step, 250 mg of MCM-41 + GPTMS was dispersed in 20 mL of EtOH and kept under constant magnetic stirring at 50 °C for 2 h. Meanwhile, a solution of succinic anhydride (Suc) in pyridine ($126 \text{ mg}\cdot\text{mL}^{-1}$) was added dropwise in a chitosan solution in HCl ($25 \text{ mg}\cdot\text{mL}^{-1}$) and was kept under stirring to ensure total solubility with strong agitation at room temperature, and then the reaction pH was adjusted to 7 using NaOH (3.0 M) aqueous solution. After that, this new solution was added dropwise to the solution of $12.5 \text{ mg}\cdot\text{mL}^{-1}$ MCM-41 + GPTMS in EtOH. This mixture was kept under constant magnetic stirring at 50 °C for 5 h. The final materials, named as MCM-41 + GPTMS + CS, were collected by centrifugation (7000 rpm) and washed thoroughly with acetone followed by vacuum drying at 37 °C for 2 days.

2.2.4. Functionalization of Mesoporous Silica MCM-41 with (3-Aminopropyl)triethoxysilane (APTES)

300 mg of MCM-41 was dispersed in 20 mL of EtOH by ultrasonication for 30 min, and the pH value was adjusted to 6–7, under magnetic stirring. Subsequently, 300 μL of APTES was dropwise added into MCM-41 in EtOH dispersion with magnetic stirring. The mixture was kept under constant magnetic stirring at 50 $^{\circ}\text{C}$ for 5 h. At the end, the suspension was filtered and washed thoroughly with Milli-Q[®] water and acetone followed by drying at 37 $^{\circ}\text{C}$ for 2 days. This sample was named MCM-41 + APTES, and it will be used as a bridge to link MCM-41 and PCL.

2.2.5. Functionalization of Mesoporous Silica MCM-41 with Poly- ϵ -caprolactone

In the next functionalization step, 7.5 $\text{mg}\cdot\text{mL}^{-1}$ of MCM-41 + APTES in EtOH was dispersed and kept under constant magnetic stirring at 50 $^{\circ}\text{C}$ for 2 h. Meanwhile, 5 $\text{mg}\cdot\text{mL}^{-1}$ of Poly- ϵ -caprolactone in acetic acid was dispersed by ultrasonication for 30 min and kept under stirring to ensure total solubility with strong agitation at room temperature, and then the reaction pH was adjusted to 7 using NaOH (3.0 M) aqueous solution. After that, this new solution was added dropwise to the solution of 7.5 $\text{mg}\cdot\text{mL}^{-1}$ MCM-41 + APTES in EtOH. This mixture was kept under constant magnetic stirring at 70 $^{\circ}\text{C}$ for 5 h. At the end, the suspension was filtered and washed thoroughly with EtOH followed by drying at 37 $^{\circ}\text{C}$ for 2 days. The final material was named as MCM-41 + APTES + PCL.

2.2.6. Physicochemical and Morphological Characterization of the MCM-41 and the Functionalized Systems

The samples were characterized using thermogravimetric analysis (TGA), Fourier transform infrared spectroscopy (FTIR), N_2 adsorption/desorption, X-ray Diffraction (XRD), scanning electron microscopy (SEM), and elemental analysis (CHN) techniques.

The weight loss of the samples was determined in a Shimadzu thermogravimetric analyzer (TGA) 50 WS. All measurements were carried out within a nitrogen atmosphere (50 $\text{mL}\cdot\text{min}^{-1}$) using (Shimadzu, Kyoto, Japan) a sample mass of approximately 4 mg from 20 to 1100 $^{\circ}\text{C}$, at 10 $^{\circ}\text{C}\cdot\text{min}^{-1}$. The typical functional groups from silica and the functionalizing agents were characterized by FTIR. The procedure was conducted in a Thermo Nicolet 6700 spectrophotometer (Waltham, MA, USA), ranging from 4000 to 400 cm^{-1} with 256 scans and 4 cm^{-1} of resolution. Nitrogen adsorption isotherms of samples were obtained using a Quantachrome Nova 2200 adsorption analyzer (Boyton Beach, FL, USA). Before the adsorption measurements, non-functionalized materials were outgassed for 4 h at 300 $^{\circ}\text{C}$, whereas the functionalized ones were outgassed for 48 h at 40 $^{\circ}\text{C}$. All data analyses were performed using the NovaWin V.10, 1997–2007 Quantachrome Instruments software (Boyton Beach, FL, USA). The specific surface areas were determined using the Brunauer–Emmett–Teller (BET) method at -196°C , and the specific pore volume and pore diameter were determined by Barrett-Joyner-Halenda (BJH) according to the manufacturer's instructions. X-ray diffraction patterns of catalysts were recorded on a Rigaku Ultima IV (Rigaku, Tokyo, Japan) diffractometer using Cu $\text{K}\alpha$ radiation as the X-ray source. SEM characterization was performed in a Carl Zeiss Field Emission Scanning Electron Microscope (ZEISS, Jena, Germany), model sigma VP equipped with an energy-dispersive X-ray (EDS). The functionalization rate was determined by elemental analyses, which were performed in a Perkin-Elmer CHNS model 2400 (Waltham, MA, USA).

2.3. Biological Assays

2.3.1. In Vitro Cytotoxicity Assays

Measurement of cell viability and proliferation forms the basis for numerous in vitro assays of a cell population's response to external factors. The reduction of tetrazolium salts is a way to examine cell proliferation. The yellow tetrazolium MTT is reduced by metabolically active cells, in part by the action of dehydrogenase enzymes to generate reducing equivalents such as nicotinamide adenine dinucleotide (NADH) and dihydronicotinamide adenine dinucleotide phosphate (NADPH).

The resulting intracellular purple formazan can be solubilized and quantified by spectrophotometric means. The MTT reagent yields low background absorbance values in the absence of cells.

All cells were grown in a humidified 5% of CO₂ at 37 °C in Dulbecco's Modified Eagle's (DMEM) medium supplemented with 10% Bovine Fetal Serum (FBS) and 1% penicillin/streptomycin and amphotericin. Upon reaching 80% confluency, cells were trypsinized, and cell viability was assessed by exclusion of Tripan blue.

The cells were plated at a density of 4×10^3 cells/well in 96-well plates in a standard growth medium and incubated for 24 h to adherence. The fibroblast cells were incubated in the growth medium containing MCM-41 + APTES + PCL and MCM-41 + GPTMS + CS nanoparticles in $100 \mu\text{g}\cdot\text{mL}^{-1}$, $75 \mu\text{g}\cdot\text{mL}^{-1}$, $50 \mu\text{g}\cdot\text{mL}^{-1}$, and $20 \mu\text{g}\cdot\text{mL}^{-1}$ concentrations for 48 h at 37 °C. Meanwhile, wells containing only the cell medium were also prepared as untreated controls. After the treatment, MTT was used as an indicator of cell viability as determined by the mitochondrial-dependent reduction to formazan. MTT ($5 \text{ mg}\cdot\text{mL}^{-1}$) was then added to the cell cultures for another 4 h at 37 °C. SDS 10% HCl was added to each well to dissolve formazan crystals, and the plate was incubated for 18 h at 37 °C. The absorbance was measured at 595 nm using a microplate reader (ELX 800 BIOTEK Instruments Inc.) (Winooski, VT, USA). The survival fraction was calculated as a percentage of the control (Absorbance in control = 100% survival). The experiments were done in triplicates. The morphological aspects of control and sample-treated fibroblasts were analyzed by observation under optical microscopy.

2.3.2. In Vitro Cellular Uptake Assays—Confocal Microscopy

The observations in the confocal microscope were made using HeLa cells incubated for 24 h for adherence. The HeLa cells were treated with $50 \mu\text{g}\cdot\text{mL}^{-1}$ of the MCM-41 + APTES + PCL and MCM-41 + GPTMS + CS. To view the entrance and pathway of the rhodamine-siRNA fluorescent (siRNArod) adsorbed onto the material by the cells, a Zeiss LSM 880 confocal microscope (Carl Zeiss, Jena, Germany) was used. The HeLa cells were seeded at density of 5×10^4 cells/well in a 6-well plate containing sterile glass sheet. After 2 h, the transfection occurred with siRNArod fluorescent. Passed at 2 h from the transfection period, the cells were washed three times with PBS and fixed with paraformaldehyde. The cells were then incubated in PBS containing 0.1% Triton X-100 (Sigma-Aldrich) for 5 min. After, this blocking was performed with 1% (*w/v*) Bovine Serum Albumin (BSA, Sigma-Aldrich) and 5% normal bovine serum in PBS. Cells were double labeled with monoclonal antibodies to α -tubulin (Sigma-Aldrich) and lamin B1 (Abcam, Cambridge, MA, USA). After washing with PBS, the cells were incubated with secondary antibodies conjugated to Alexa 488 and 647 and the nuclear dye Hoechst 33258 (Life Technologies, Carlsbad, CA, USA). Then, the cells were washed again with PBS and in each well was added Prolong Gold Antifade reagent (Life Technologies). The coverslips containing the cells were assembled into Prolong Gold Antifade reagent (Life Technologies).

3. Results and Discussion

3.1. Thermogravimetric Analysis—TGA

The amount of organic moieties loaded in the MSNs host was determined by thermogravimetry. The TGA curves of all the systems are shown in Figure 1. The weight losses of MCM-41 and functionalized samples were evaluated in the range of 25–800 °C and are shown in Table 1. The TGA pattern of MCM-41 demonstrates one weight loss around 12.6% from environment temperature to 150 °C that was attributed to the thermodesorption of physically adsorbed water, Figure 1. Above this temperature and up to 800 °C, no significant weight loss is verified. In this temperature range, a small weight loss of approximately 3.9% was attributed to the decomposition of residual CTAB surfactant. The total weight loss above 650 °C was 16.5% for pure MCM-41. Studies carried out by Mintzer, and Simanek and Freitas et al., reported similar results to those reported in previous publications [18–20].

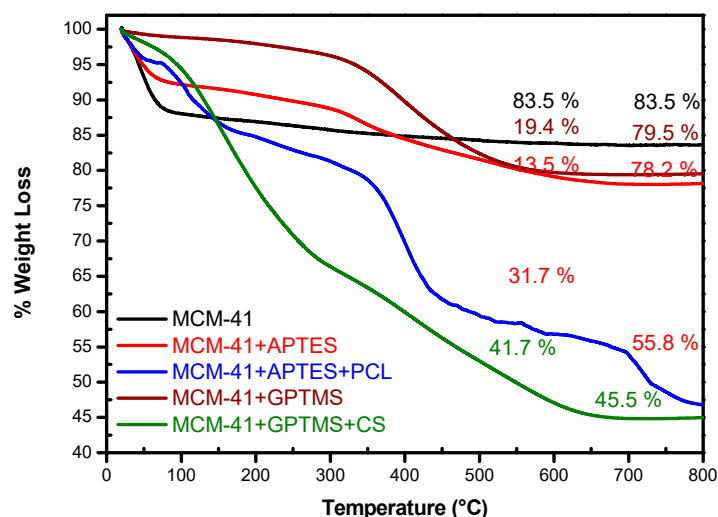


Figure 1. TGA analysis of pure MCM-41 and modified samples with APTES-PCL and GPTMS-CS.

Table 1. TGA analysis of pure and functionalized MCM-41 samples.

Samples	Weight Loss (% W/W)		Residues > 650 °C (% W/W)
	20–150 °C	150–650 °C	
MCM-41	12.6	3.9	83.5
MCM-41 + APTES	8.5	13.5	78.2
MCM-41 + APTES + PCL	12.5	31.7	55.8
MCM-41 + GPTMS	1.5	19.4	79.1
MCM-41 + GPTMS + CS	13.1	41.7	45.2

In case of the functionalized samples, weight loss occurred in distinct regions. The functionalization with APTES that reacted with the silanol groups adding amino groups on the surface of the MCM-41, shows, in TGA analysis, a weight loss of 8.5% in range of 20 °C and 150 °C, Figure 1. A lower percentage of mass loss is observed in functionalized samples, and a lower water adsorption of these samples can be attributed. This is due to the decrease of free hydroxyl groups present on the surface of the sample when it is chemically modified. Furthermore, MCM-41 was functionalized with groups that promoted a non-polar silica scale. As a consequence, the loss of mass in the first region is much lower for a functionalized than for a pure sample due to surface hydration. In temperature range between 150 °C and 650 °C, this sample loses 13.5% weight, which indicates the total decomposition of the amino groups anchored on the MSNs surface. The residual mass for this sample is 78%; the results indicate that APTES had been successfully grafted onto the surface of MCM-41.

The crosslink APTES serve as bridge between PCL and MCM-41 nanoparticles for the surface functionalization of MCM-41 + APTES with PCL, enhancing the interfacial adhesion between the two phases, adding new functional groups to MCM-41. As shown in TGA analysis, a loss weight of 31.7% could be observed in range between 150 °C and 650 °C, indicating the decomposition of the PCL organic material onto the surface of the MCM-41 + APTES, as can be observed in Figure 1.

The TGA curves of MCM-41 + GPTMS and MCM-41 + GPTMS + CS samples are shown in Figure 1, and their percentages of weight loss are shown in Table 1. The functionalization with GPTMS, which reacted with the silanol groups on the surface of the MCM-41 adding epoxy groups, owing to the characteristic by new functional groups to MCM-41, and samples grafted with CS shows, in TGA analysis, similar behavior to that observed for PCL functionalized samples. In temperature range between 150 °C and 650 °C, this sample loses 19.4% weight, which indicates the total decomposition of the epoxy and glycidoxypropyl groups as related by Hoşgör et al. [21]. This result indicated that GTPMS had been successfully grafted onto the surface of the MCM-41.

The MCM-41 + GPTMS surface functionalization with CS, shown in TGA analysis, a weight loss of 13.1% in range between 20 °C and 150 °C; between 150 °C and 650 °C, this sample lost 41.7% weight and the total weight loss in temperature above 650 °C was 54.8%, and the residual mass was 45.2%, indicating the decomposition of CS-Suc coating onto the surface of the MCM-41 + GPTMS. TGA results may be associated with the degradation of the polymer chains from MSN surface.

3.2. Fourier Transform Infrared Spectroscopy—FTIR

FTIR spectra are a useful tool with which to identify the presence of functional groups in compounds according to the each specific chemical bond. Figure 2 shows the FTIR spectra of MCM-41, MCM-41 + APTES, and MCM-41 + APTES + PCL samples. Spectrum of MCM-41 shows peak of hydroxyl stretching band for both silanol Si–O–H and the water hydroxyls at 3465 cm^{-1} , in addition to the peak of H–OH water twisting band at 1640 cm^{-1} . The Si–O vibration and Si–O bond stretching of surface Si–OH groups are shown at 1090 cm^{-1} and 967 cm^{-1} , respectively, indicating that they are mainly composed of a silica network [21].

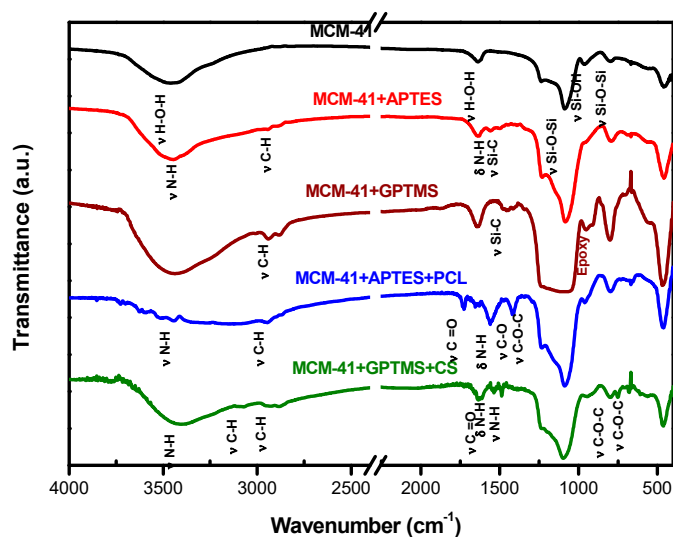


Figure 2. FTIR analysis of pure MCM-41 and modified samples with APTES-PCL and GPTMS-CS.

For functionalized samples, additional peaks can be observed; in the first step, in which APTES was grafted into MCM-41 surface, peaks are observed at 2963 cm^{-1} and 2886 cm^{-1} due to stretching vibration of C–H bond and a peak is observed at 1569 cm^{-1} related to the N–H deformation modes of the amine groups, as expected after the amination process [22]. There is a modification in the 950 cm^{-1} peak (Si–OH), showing less definition than in the MCM-41 spectrum. This result indicates that APTES has grafted successfully into the surfaces of the MCM-41.

The spectrum of the second step of functionalization, which refers to surface modification, revealed typical peak for PCL related to 2963 cm^{-1} and 2886 cm^{-1} due to stretching vibration of C–H bond, peak at 1723 cm^{-1} related to stretching vibration of C=O, and asymmetric and symmetric C–O–C stretching vibration around 1240 cm^{-1} and 1160 cm^{-1} , respectively, as related in the literature [23,24].

In addition to the bands related to the fundamental functional groups of the silica, the CS functionalized silica samples presented other bands that are assigned to the organic groups bonded to the material surface, as shown in Figure 2. For MCM-41 + GPTMS and MCM-41 + GPTMS + CS samples, additional peaks can be observed; in the first step, in which GPTMS was anchored into MCM-41 surface, the presence of peaks at 2940 cm^{-1} and 2860 cm^{-1} due to stretching vibration of C–H bond are observed. Indeed, the peak at 1445 cm^{-1} corresponding to Si–C bond stretching present on glycidoxypropyl group, and the peak at 901 cm^{-1} due to epoxy group, are identified, indicating that GPTMS has grafted successfully onto the surfaces of the MCM-41 as related in [25].

The spectrum of the second step of functionalization, which refers to surface modification with chitosan-succinate, revealed typical peaks at 3068 cm^{-1} , 2940 cm^{-1} , and 2860 cm^{-1} due to stretching vibration of C–H bond. Carboxylic carbonyl stretching in the range of peaks at $1710\text{--}1720\text{ cm}^{-1}$ is identified, indicating the formation of amide links with succinate moieties. Moreover, the presence of peak around $1660\text{--}1670\text{ cm}^{-1}$ could be observed, which was attributed to amide carbonyl stretching, the peak of 1536 cm^{-1} due to the deformation of N–H (Amine I), the peak of 1467 cm^{-1} belonging to the stretching vibration of N–H (amide III), and peaks at 750 cm^{-1} and 680 cm^{-1} due to stretching vibration of C–O–C bond from the saccharide structure β 1-4 as related in [26].

Therefore, the FTIR results demonstrate that organic moieties have been successfully grafted onto the MCM-41 surface.

3.3. Nitrogen Adsorption/Desorption

The physical properties of these MSNs like pore volume, pore size distribution, and specific surface area were measured by N_2 adsorption–desorption. The surface area of MCM-41, pore volume, and pore size decreased as the extent of modification increased by different steps of functionalization, as shown in Table 2.

Table 2. N_2 adsorption/desorption analysis of pure MCM-41 and modified samples.

Samples	S_{BET} ($\text{m}^2\cdot\text{g}^{-1}$)	V_P ($\text{cm}^3\cdot\text{g}^{-1}$)	D_P (nm)
MCM-41	987.0	0.299	3.3
MCM-41 + APTES	325.2	0.228	3.8
MCM-41 + APTES + PCL	45.9	0.152	3.0
MCM-41 + GPTMS	411.8	0.252	3.3
MCM-41 + GPTMS + CS	12.0	0.116	3.3

MCM-41 exhibited a sharp step of capillary condensation in primary mesopores at the relative pressure range $0.2 < P/P_0 < 0.4$, indicating the narrow pore size distribution of the material.

The adsorption and desorption isotherms of N_2 on sample MCM-41 show the typical type IV isotherm according to the IUPAC nomenclature (Figure 3). At the adsorption branch, the adsorbed amount increased gradually with an increase in relative pressure by adsorption. The desorption branch of the isotherm coincides with the adsorption branch, and the surface area is $987.0\text{ m}^2\cdot\text{g}^{-1}$ (Table 2).

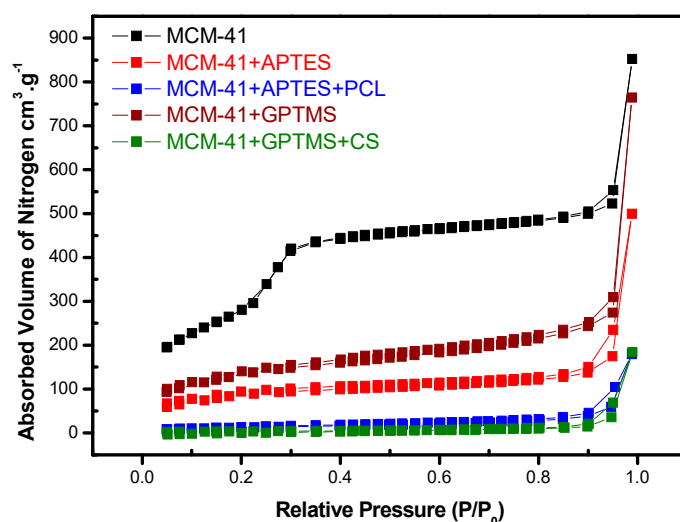


Figure 3. N_2 adsorption–desorption isotherms of pure MCM-41 modified with APTES-PCL and GPTMS-CS samples.

The functionalization of the surfaces of MCM-41 with APTES leads to a decrease in the surface area ($352.2 \text{ m}^2 \cdot \text{g}^{-1}$); the same is observed in the functionalization of the surfaces of MCM-41 + APTES with PCL ($45.9 \text{ m}^2 \cdot \text{g}^{-1}$). This decrease evidences that the pore wall is indeed covered by organic moieties added in different steps of chemical modifications. Correspondingly, a decrease of pore volume of 0.299 to $0.152 \text{ cm}^3 \cdot \text{g}^{-1}$ is observed, which is evidence that organic material is also located within the pores of the matrices (Table 2). So, after modification, the surface area and pore volume decreased significantly. The extent of such a decrease was dependent on the size of bonded groups, which is expected. These results are in line with reported by Lara et al. [20].

Similar behavior was observed for samples modified with GPTMS and CS, as shown in Figure 3 and Table 2. The functionalization of the surfaces of MCM-41 with GPTMS leads to a decrease in the surface area ($411.8 \text{ m}^2 \cdot \text{g}^{-1}$); the same is observed in the functionalization of the surfaces of MCM-41 + GPTMS with CS ($12.0 \text{ m}^2 \cdot \text{g}^{-1}$). This decrease evidences that the pore wall is indeed covered by organic moieties added in different steps of chemical modifications. Correspondingly, a decrease of pore volume of 0.299 to $0.116 \text{ cm}^3 \cdot \text{g}^{-1}$ is observed, which is evidence that the organic material is also located within the pores of the matrices (Table 2).

3.4. Elemental Analysis—CHN

The CHN analysis of bare MSNs matrices and the functionalized ones were used to quantify the organic molecules anchored to its surfaces. The results are shown in Table 3. The carbon and nitrogen concentrations of functionalized MSNs increased significantly in relation to the bare MSNs, indicating that the bare matrices were successfully functionalized; these results are in line with reports in literature [17,19].

Table 3. Elemental analysis of MCM-41 and its modified surface samples.

Samples	C (%)	Δ C (%)	H (%)	Δ H (%)	N (%)	Δ N (%)
MCM-41	-	-	1.26	-	-	-
MCM-41 + APTES	8.44	8.44	2.99	1.73	3.20	3.20
MCM-41 + APTES + PCL	24.46	16.02	4.62	1.63	2.33	-
MCM-41 + GPTMS	2.0	2.0	2.80	1.54	-	-
MCM-41 + GPTMS + CS	18.8	16.8	2.80	-	3.20	3.20

MCM-41 + APTES sample presents elemental contents of 8.44% of carbon, 2.99% of hydrogen, and 3.2% of nitrogen. The increasing percentages of carbon, hydrogen, and nitrogen are due to presence of aminopropyl groups functionalized in MCM-41, which is in line with [19,20].

The 24.66%, 4.62%, and 2.33% of carbon, hydrogen, and nitrogen, respectively, are the percentages relative to MCM-41 + APTES + PCL sample. They show the increase of carbon and hydrogen, which proves that the PCL was successfully anchored on MCM-41 nanoparticles. The PCL consists of 63.08% of carbon and 9.43% of hydrogen, and these results are consistent with FTIR analyses that shows the peaks bands related to PCL and the BET analyses that show a decrease of surface area, suggesting that the PCL is anchored on MCM-41.

In MCM-41 + GPTMS sample, an increase of 2.0% of carbon and 2.8% of hydrogen is observed. Combining this result with FTIR data, which shows the presence of peak bands of epoxy groups from GPTMS, it is possible to suggest that samples were successfully functionalized with this organic group.

The 18.7%, 2.8%, and 3.2% content of carbon, hydrogen, and nitrogen, respectively, shows the concentration increase of these elements, which demonstrates that the CS was successfully anchored on MCM-41 nanoparticles. The amino groups present in the structure of CS are related by the increase of nitrogen, and are in agreement with the BET analysis that shows the decrease of surface area, indicating the success of functionalizing matrices.

3.5. X-ray Diffraction—XRD

The XRD diffraction patterns (Figure 4) show two characteristic peaks at angles $2\theta = 21.4^\circ$ and 23.8° , corresponding to the (110) and (200) crystallographic planes of semi-crystalline nature of PCL [27] anchored in the structure of functionalized MCM-41 nanoparticles. These two peaks characteristic of PCL observed in this nanoparticle indicate miscibility among the nanoparticles and PCL, which means that the functionalization with PCL occurs successfully in the presence of the crystalline structure of PCL. The MCM-41 and MCM-41 + APTES nanoparticles do not present crystallographic planes, indicating the absence of the crystalline structure and, therefore, the presence of an amorphous structure.

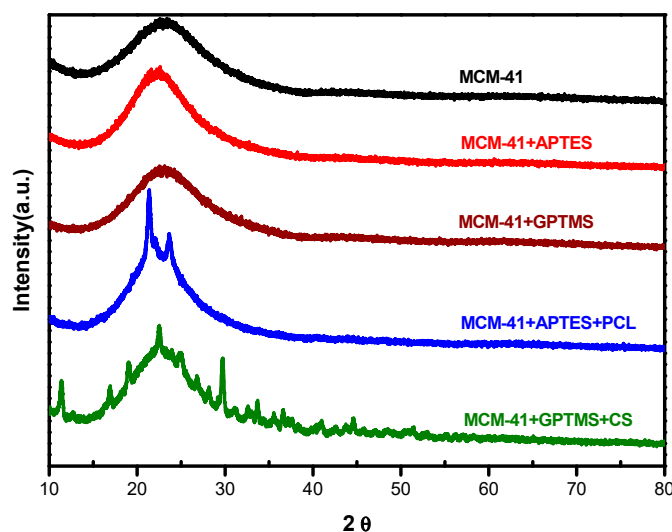


Figure 4. XRD of pure MCM-41 modified with APTES-PCL and GPTMS-CS surface samples.

As reported by Islam et al. [28], the XRD pattern of Chitosan shows diffraction peaks at $2\theta = 10^\circ$ and 21° that indicate semi-crystalline structure; similar peaks are observed for MCM-41 + GPTMS + CS sample; probably, the effect of succinic anhydride in nanoparticles appeases the formation of a semi-crystalline structure of MCM-41 + GPTMS + CS sample (Figure 4).

3.6. Scanning Electron Microscopy—SEM

The morphological characterization of silica nanoparticles was carried out using SEM technique. Images of MCM-41 showed spherical morphology of most nanoparticles and low heterogeneity among them (Figure 5). As estimated by the Quantikov Image Analyzer data [29], the particles present an average mean diameter of approximately 110 ± 20 nm (in a total of 161 measurements). As can be seen, the spherical shape was not altered by the presence of organic moieties (Figure 5b,c), although the particle size distribution was slightly modified.

In the case of MCM-41 + APTES + PCL sample (Figure 5b), the histogram shows an average diameter of 130 nm (in a total of 124 measurements) and the histogram of MCM-41 + GPTMS + CS sample (Figure 5c) shows an average diameter of 185 nm (in a total of 75 measurements). The functionalization process with APTES + PCL and GPTMS + CS increased the size of MCM-41 nanoparticles. The MCM-41 nanoparticles have large surface areas and pore volumes that enable the encapsulation and delivery of large quantities of organic molecules through different cell membranes. Furthermore, it has been demonstrated that the mesopores of these nanoparticles can be closed by APTES + PCL, GPTMS + CS, and their surfaces with the same organic matrices capping. As reported by Liberman et al. [30], the presence of organic moieties in the surface increased the shapes and sizes of nanoparticles. It is worth mentioning that the MCM-41 is within the size expected to be used in biological applications.

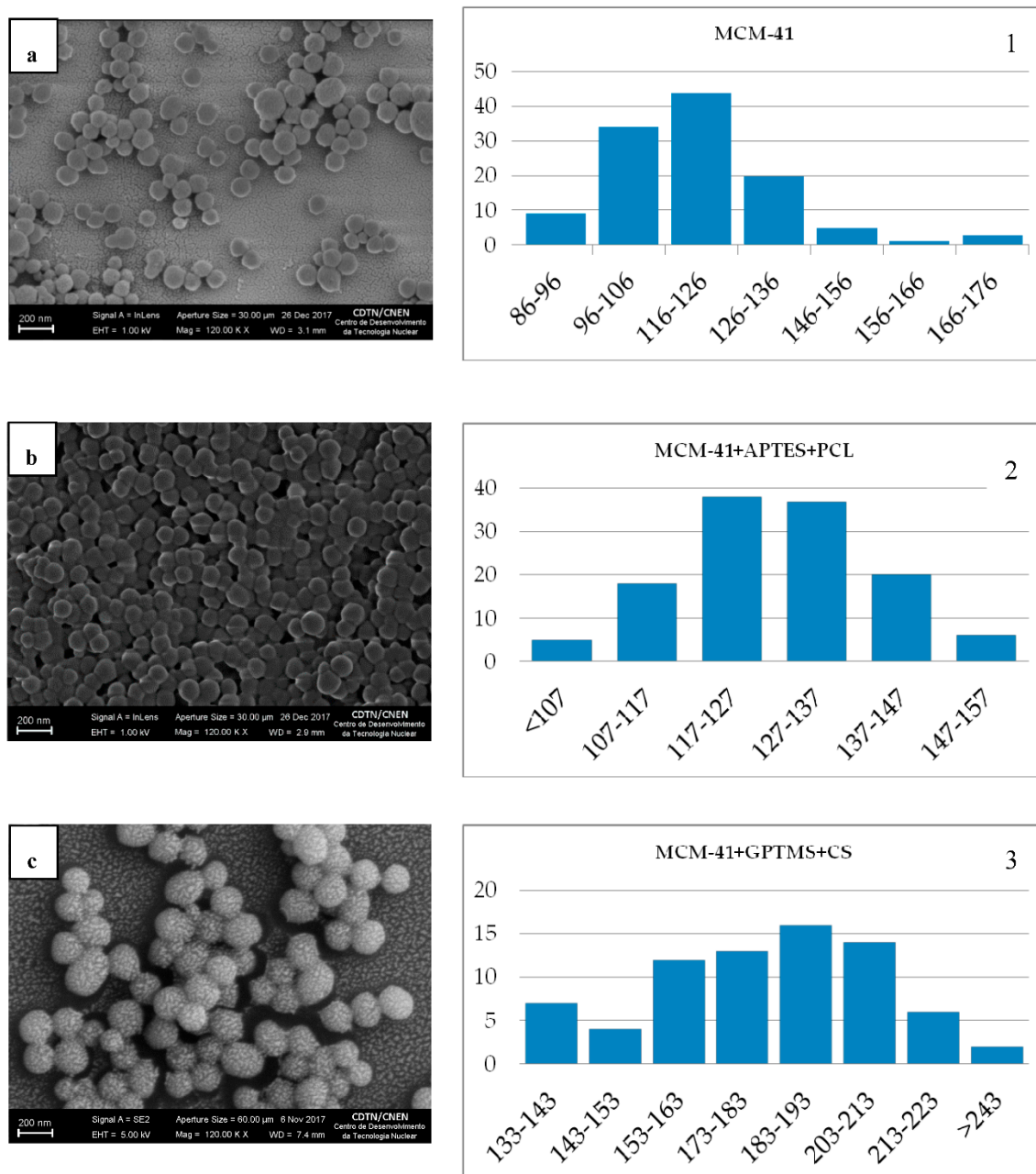


Figure 5. SEM image of (a) MCM-41, (b) MCM-41 + APTES + PCL, and (c) MCM-41 + GPTMS + CS samples and its histogram size distribution of (1) MCM-41; (2) MCM-41 + APTES + PCL and (3) MCM-41 + GPTMS + CS.

3.7. Biological Assays

3.7.1. Cellular Viability

The cytotoxicity is evaluated by MTT assay using fibroblast cell line. As shown in Figure 6, the fibroblast cells were treated with MCM-41 + APTES + PCL and MCM-41 + GPTMS + CS, and nanoparticles in $100 \mu\text{g}\cdot\text{mL}^{-1}$, $75 \mu\text{g}\cdot\text{mL}^{-1}$, $50 \mu\text{g}\cdot\text{mL}^{-1}$, and $20 \mu\text{g}\cdot\text{mL}^{-1}$ concentrations were evaluated. More than 90% of the fibroblast cells are still viable in all concentrations used and showed little statistical difference between MCM-41 + APTES + PCL and MCM-41 + GPTMS + CS nanoparticles, as shown in Figure 6. The results indicate that nanoparticles have good biocompatibility.

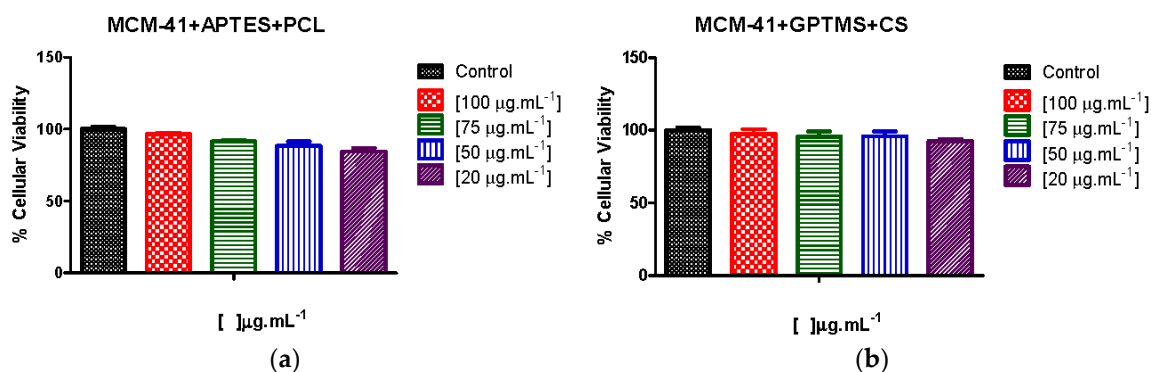


Figure 6. The MTT assays in vitro of cytotoxicity and biocompatibility of different nanoparticles. (a) MCM-41 + APTES + PCL; (b) MCM-41 + GPTMS + CS.

These results indicate that MCM-41 + APTES + PCL and MCM-41 + GPTMS + CS nanoparticles have potential to be used as nonviral vectors. As reported by others authors [26] using chitosan-silica hollow nanospheres as promising drug nanocarriers consisting of mono-dispersed and pH sensitive suitable for breast cancer therapy, which used concentrations above $100 \mu\text{g}\cdot\text{mL}^{-1}$, significant cytotoxicity against the breast cancer cell line (MCF-7 cells) was not shown. As described by Hu et al. [31], chitosan-capped nanoparticles as pH-Responsive nanocarriers for controlled drug release can exhibit perfect biocompatibility in concentrations above $100 \mu\text{g}\cdot\text{mL}^{-1}$.

Thus, the concentrations of nanoparticles that we used in this work are considered ideal for biological applications.

We analyzed the effect of organic molecules on surface of MCM-41. As reported by Kim et al. [32], the APTES functionalized in nanoparticles were complexed with bone morphogenetic protein-2 (BMP2) plasmid DNA (pDNA) to transfection efficiency in mesenchymal stem cells. The results showed that in concentrations above $100 \mu\text{g}\cdot\text{mL}^{-1}$, the presence of APTES is toxic with 50% of viable cells. Other results report [33] using APTES modified nanoparticles to form dsDNA (double-stranded DNA) complexes, showing that even at a concentration above of $100 \mu\text{g}\cdot\text{mL}^{-1}$, the presence of APTES is not toxic with 80% of viable cells. Probably, the toxicity of APTES depends on the cell line. Thus, in this work, the presence of APTES in nanoparticles did not affect cellular viability, and it is considered model for biological applications.

Both PCL and CS are biodegradable cationic polymers, which easily anchor onto surfaces of MCM-41, enhancing the biocompatibility and its presence on the structure of MCM-41, which did not affect the cellular viability as reported in [31,33].

3.7.2. In Vitro Cellular Uptake Assays

In order to investigate the cellular uptake in HeLa cells, the immunofluorescence assay with confocal microscopy image was used, as shown in Figure 7. It was observed by the results obtained in the cell viability assay that in concentration of $50 \mu\text{g}\cdot\text{mL}^{-1}$ of MCM-41 + APTES + PCL, nanoparticles had high viable cells, which made them favorable for use. We observed the intracellular transport of the nanoparticles by rhodamine-siRNA fluorescent (siRNARod) incorporated in the MCM-41 + APTES + PCL nanoparticles. Cells were labeled with specific antibodies against α -tubulin, a cytoskeletal protein and lamin B1, a nuclear membrane marker to identify the cytosolic and nuclear compartments. The rhodamine-siRNA-MCM-41 + APTES + PCL nanoparticles are bounded and taken up by cells, as shown by fluorescent emission of these nanoparticles.

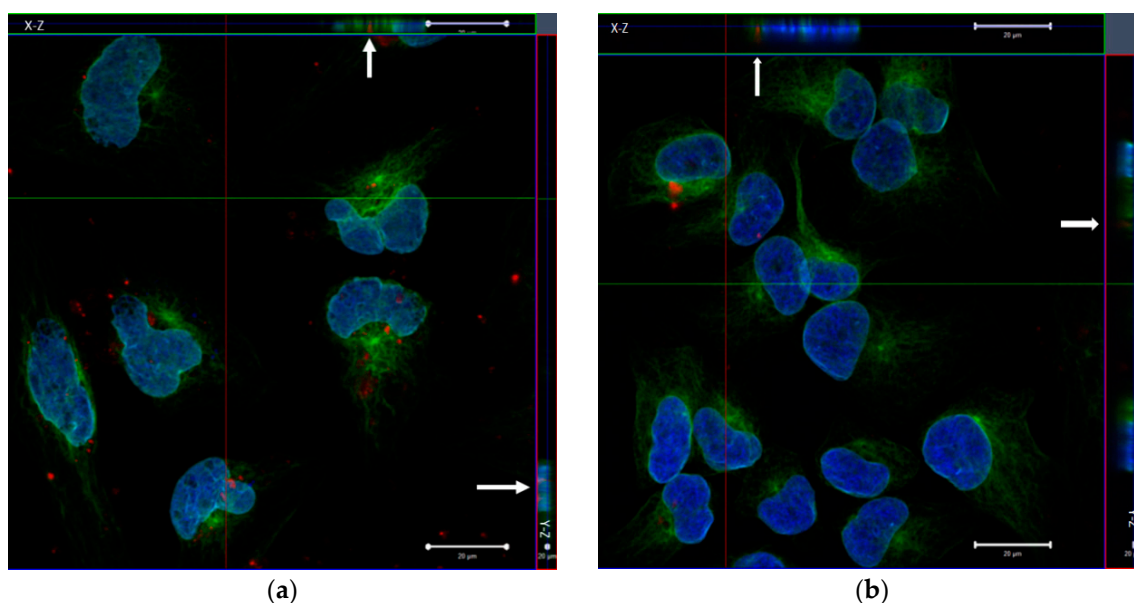


Figure 7. Cellular internalization of siRNA-MCM-41 + APTES + PCL conjugates. Rhodamine-siRNA-MCM-41 + APTES + PCL is in red, α -tubulin is in green, Lamin B1 is in cyan, and nucleus is stained with Hoechst in blue. Representative image of serial optical sections collected for three-dimensional reconstruction; x-z sections are shown at the top, and y-z sections are shown at the right of image. siRNA-MCM-41 + APTES + PCL co-localizes with α -tubulin, as indicated by yellow overlay (White arrows). Scale bar = 20 μm . (a) Cellular uptake of fluorescent rhodamine-siRNA-MCM-41 + APTES + PCL in HeLa cells; (b) Cellular uptake of fluorescent rhodamine-siRNA-MCM-41 + APTES + PCL in HeLa cells in another field.

The three-dimensional reconstruction of serial confocal immunofluorescence images revealed the intracellular complex localization. Co-localization of rhodamine-siRNA-MCM-41 + APTES + PCL α -tubulin (green) was demonstrated by the appearance of the color yellow (Figure 7). Together, these findings indicate the internalization and cytosolic localization of MCM-41 + APTES + PCL nanoparticles.

As expected, the surface amino groups allowed for an attractive interaction with the negatively charged siRNA rod; in other words, the high positive charge of MCM-41 + APTES + PCL nanoparticles was beneficial for nucleic acid adsorption capacity according to Zhang et al. [34]. According to Xia et al. [35], PCL showed a lower cytotoxicity and a higher transfection efficiency in HeLa cells, and there was no decrease of the transfection efficiency. These characteristics are favorable for application as gene delivery systems.

The entry of the MCM-41 + APTES + PCL nanoparticles into the cells is evident, since siRNA is adsorbed in these nanoparticles, and it does not cross the cell membrane alone. It was shown that siRNA trapped inside the PCL-coated MCM-41 was efficiently protected against enzymatic degradation. The siRNA could be released into the cytoplasm and escape from the MCM-41 after MCM-41 internalization by A549 cells, as evidenced by fluorescently labeled siRNA and MCM-41 and efficiently knocked-down target genes [35]. According to Zhang et al. [36], the siRNA can only be released through systemic delivery using nanoparticles, and it is not readily internalized by cells due to their negative charge (they suffer from poor biological stability and a short half-life).

The same was done for the packaging of siRNA into the $50 \mu\text{g}\cdot\text{mL}^{-1}$ of MCM-41 + GPTMS + CS nanoparticles. As shown in Figure 8, by fluorescent confocal microscopy, fluorescence patterns show the gene transfection in the $50 \mu\text{g}\cdot\text{mL}^{-1}$ of MCM-41 + GPTMS + CS nanoparticles. Probably, the siRNA was not being fully protected against degradation by nucleases. As reported in others works [37,38], the Chitosan is considered to be a good candidate for a gene delivery carrier with its excellent

biocompatibility, biodegradability, low toxicity, and high cationic potential. However, this material shows low transfection efficiency, and it may have been affected by some factors, including chitosan molecular weight, salt form, degree of deacetylation, the pH of the culture medium, and so forth.

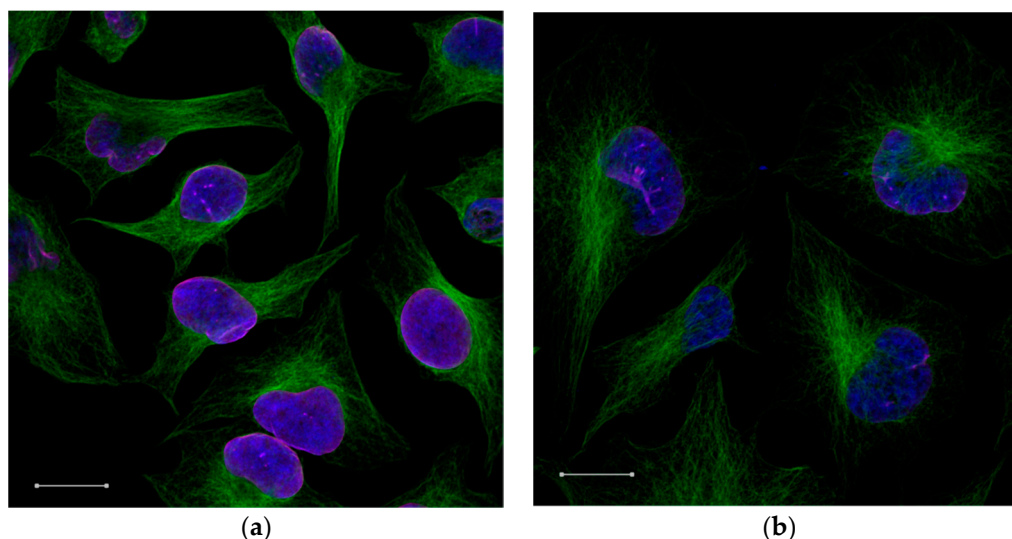


Figure 8. Fluorescent confocal laser scanning microscopic images were not able to observe the intracellular transport of siRNArod fluorescent incorporated in the MCM-41 + GPTMS + CS nanoparticles in HeLa cells. (a) Absence of cellular uptake of fluorescent rhodamine-siRNA-MCM-41 + GPTMS + CS in HeLa cells; (b) Absence of cellular uptake of fluorescent rhodamine-siRNA-MCM-41 + GPTMS + CS in HeLa cells in another field.

4. Conclusions

This study was able to show the surface modification process of MCM-41 with two biodegradable polymers to act as nonviral gene delivery in HeLa cells. The physical–chemical and morphological characterizations, as well as the applicability of functionalized MCM-41 as platforms for gene delivery, were assessed. The results confirmed that MCM-41 was successfully functionalized with PCL, and CS kept its typical morphology and pore arrangement.

MTT analysis in the fibroblast cell line indicated that the presence of materials in concentrations up to $100 \mu\text{g}\cdot\text{mL}^{-1}$ did not compromise the cell metabolism and, consequently, cell viability. The results confirmed that MCM-41 functionalized with PCL can effectively be used as a nonviral vector in gene delivery systems. The MCM-41 functionalized with CS shows inefficient gene unpacking and therefore low gene transfection efficiency compared with MCM-41 functionalized with PCL. These results are promising for the use of these nanoparticles as siRNA delivery nonviral vectors.

Author Contributions: E.M.B.d.S. and E.P.F.N. conceived of and designed the experiments and analyzed the data. E.P.F.N. performed the preparation, characterization, and the whole experiment of functionalized samples. G.F.A. and J.A.Q.A.F. performed the biological assays, and D.A.G. wrote the biological results parts. All authors read and approved the final manuscript.

Acknowledgments: The authors wish to thank FAPEMIG (Fundação de Amparo a Pesquisa do Estado de Minas Gerais), CNPQ (Conselho Nacional de Desenvolvimento Científico e Tecnológico), and CAPES (Comissão Aperfeiçoamento de Pessoal de Nível Superior) for their financial support.

Conflicts of Interest: The authors declare no conflict of interest.

References

1. Zhou, Y.; Quan, G.; Wu, Q.; Zhang, X.; Niu, B.; Wu, B.; Huang, Y.; Pan, X.; Wu, C. Mesoporous silica nanoparticles for drug and gene delivery. *Acta Pharm. Sin. B* **2018**, *8*, 165–177. [[CrossRef](#)] [[PubMed](#)]
2. Beck, J.S.; Vartuli, J.C.; Roth, W.J.; Leonowicz, M.E.; Kresge, C.T.; Schmitt, K.D.; Chu, C.T.W.; Olson, D.H.; Sheppard, E.W.; McCullen, S.B.; et al. A New Family of Mesoporous Molecular Sieves Prepared with Liquid Crystal Templates. *J. Am. Chem. Soc.* **1992**, *114*, 10834–10843. [[CrossRef](#)]
3. Kresge, C.T.; Leonowicz, M.E.; Roth, W.J.; Vartuli, J.C.; Beck, J.S. Ordered mesoporous molecular sieves synthesized by a liquid-crystal template mechanism. *Nature* **1992**, *359*, 710–712. [[CrossRef](#)]
4. Kwon, S.; Singh, R.K.; Perez, R.A.; Neel, E.A.A.; Kim, H.-W.; Chrzanowski, W. Silica-based mesoporous nanoparticles for controlled drug delivery. *J. Tissue Eng.* **2013**, *4*, 204173141350335. [[CrossRef](#)] [[PubMed](#)]
5. Kankala, R.K.; Kuthati, Y.; Liu, C.-L.; Mou, C.-Y.; Lee, C.-H. Killing cancer cells by delivering a nanoreactor for inhibition of catalase and catalytically enhancing intracellular levels of ros. *RSC Adv.* **2015**, *5*, 86072–86081. [[CrossRef](#)]
6. Kankala, R.K.; Liu, C.-G.; Chen, A.-Z.; Wang, S.-B.; Xu, P.-Y.; Mende, L.K.; Liu, C.-L.; Hung, C.-H.; Hu, Y.-F. Overcoming Multidrug Resistance through the Synergistic Effects of Hierarchical pH-Sensitive, ROS-Generating Nanoreactors. *ACS Biomater. Sci. Eng.* **2017**, *3*, 2431–2442. [[CrossRef](#)]
7. Slita, A.; Egorova, A.; Casals, E.; Kiselev, A.; Rosenholm, J.M. Characterization of modified mesoporous silica nanoparticles as vectors for siRNA delivery. *Asian J. Pharm. Sci.* **2018**. [[CrossRef](#)]
8. Manzano, M.; Aina, V.; Areán, C.O.; Balas, F.; Cauda, V.; Colilla, M.; Delgado, M.R.; Vallet-Regí, M. Studies on mcm-41 mesoporous silica for drug delivery: Effect of particle morphology and amine functionalization. *Chem. Eng. J.* **2008**, *137*, 30–37. [[CrossRef](#)]
9. Hung, B.-Y.; Kuthati, Y.; Kankala, R.; Kankala, S.; Deng, J.-P.; Liu, C.-L.; Lee, C.-H. Utilization of enzyme-immobilized mesoporous silica nanocontainers (ibn-4) in prodrug-activated cancer theranostics. *Nanomaterials* **2015**, *5*, 2169–2191. [[CrossRef](#)] [[PubMed](#)]
10. Milgroom, A.; Intrator, M.; Madhavan, K.; Mazzaro, L.; Shandas, R.; Liu, B.; Park, D. Mesopores silica nanoparticles as a breast cancer targeting ultrasound agent. *Colloids Surf. B Biointerfaces* **2014**, *116*, 652–657. [[CrossRef](#)] [[PubMed](#)]
11. Lu, J.; Liong, M.; Zink, J.I.; Tamanoi, F. Mesopores silica nanoparticles as a delivery system for hydrophobic anticancer drug. *Small* **2007**, *3*, 1341–1346. [[CrossRef](#)] [[PubMed](#)]
12. Meng, H.; Liong, M.; Xia, T.; Li, Z.; Ji, Z.; Zink, J.I.; Nel, A.E. Engineered design of mesoporous silica nanoparticles to deliver doxorubicin and p-glycoprotein sirna to overcome drug resistance in a cancer cell line. *ACS Nano* **2010**, *4*, 4539–4550. [[CrossRef](#)] [[PubMed](#)]
13. Hu, W.-W.; Elkasabi, Y.; Chen, H.-Y.; Zhang, Y.; Lahann, J.; Hollister, S.J.; Krebsbach, P.H. The use of reactive polymer coatings to facilitate gene delivery from poly (ϵ -caprolactone) scaffolds. *Biomaterials* **2009**, *30*, 5785–5792. [[CrossRef](#)] [[PubMed](#)]
14. Park, E.K.; Kim, S.Y.; Lee, S.B.; Lee, Y.M. Folate-conjugated methoxy poly(ethylene glycol)/poly(epsilon-caprolactone) amphiphilic block copolymeric micelles for tumor-targeted drug delivery. *J. Control. Release* **2005**, *109*, 158–168. [[CrossRef](#)] [[PubMed](#)]
15. Pillai, C.K.S.; Paul, W.; Sharma, C.P. Chitin and chitosan polymers: Chemistry, solubility and fiber formation. *Prog. Polym. Sci.* **2009**, *34*, 641–678. [[CrossRef](#)]
16. Chen, Y.; Xu, G.; Zheng, Y.; Yan, M.; Li, Z.; Zhou, Y.; Mei, L.; Li, X. Nanoformulation of D- α -tocopheryl polyethylene glycol 1000 succinate-b-poly (ϵ -caprolactone-ran-glycolide) diblock copolymer for siRNA targeting HIF-1 α for nasopharyngeal carcinoma therapy. *Int. J. Nanomed.* **2015**, *10*, 1375–1386.
17. De Oliveira Freitas, L.B.; Bravo, I.J.G.; de Almeida Macedo, W.A.; de Sousa, E.M.B. Mesoporous silica materials functionalized with folic acid: Preparation, characterization and release profile study with methotrexate. *J. Sol-Gel Sci. Technol.* **2016**, *77*, 186–204. [[CrossRef](#)]
18. Mintzer, M.A.; Simanek, E.E. Nonviral Vectors for Gene Delivery. *Chem. Rev.* **2008**, *109*, 259–302. [[CrossRef](#)] [[PubMed](#)]
19. De Oliveira Freitas, L.B.; de Melo Corgosinho, L.; Faria, J.A.Q.A.; dos Santos, V.M.; Resende, J.M.; Leal, A.S.; Gomes, D.A.; de Sousa, E.M.B. Multifunctional mesoporous silica nanoparticles for cancer-targeted, controlled drug delivery and imaging. *Microporous Mesoporous Mater.* **2017**, *242*, 271–283. [[CrossRef](#)]

20. Nanoparticles, A.M.; Lara, G.G.; Fernandes, M.; Id, C.; Andrade, G.F. Response of Fibroblasts MRC-5 to Flufenamic Acid-Grafted MCM-41 Nanoparticles. *Bioengineering* **2018**, *5*, 4.
21. Hoşgör, Z.; Apohan, N.K.; Karatas, S.; Menceloğluc, Y.; Güngör, A. Preparation and characterization of phosphine oxide based polyurethane/silica nanocomposite via non-isocyanate route. *Prog. Organ. Coat.* **2010**, *69*, 366–375. [[CrossRef](#)]
22. Joseph, T.; Kumar, K.V.; Ramaswamy, A.V.; Halligudi, S.B. Au-Pt nanoparticles in amine functionalized MCM-41: Catalytic evaluation in hydrogenation reactions. *Catal. Commun.* **2007**, *8*, 629–634. [[CrossRef](#)]
23. Liverani, L.; Lacina, J.; Roether, J.A.; Boccardi, E.; Killian, M.S.; Schmuki, P.; Schubert, D.W.; Boccaccini, A.R. Incorporation of bioactive glass nanoparticles in electrospun PCL/chitosan fibers by using benign solvents. *Bioact. Mater.* **2018**, *3*, 55–63. [[CrossRef](#)] [[PubMed](#)]
24. Liverani, L.; Boccardi, E.; Beltran, A.M.; Boccaccini, A.R. Incorporation of calcium containing mesoporous (MCM-41-type) particles in electrospun PCL fibers by using benign solvents. *Polymers* **2017**, *9*, 487. [[CrossRef](#)]
25. Chen, S.; You, B.; Zhou, S.; Wu, L. Preparation and characterization of scratch and mar resistant waterborne epoxy/silica nanocomposite clearcoat. *Appl. Polym.* **2009**, *112*, 3634–3639. [[CrossRef](#)]
26. Pereira, V.A.; de Arruda, I.N.Q.; Stefani, R. Active chitosan/PVA films with anthocyanins from Brassica oleraceae (Red Cabbage) as Time-Temperature Indicators for application in intelligent food packaging. *Food Hydrocoll.* **2015**, *43*, 180–188. [[CrossRef](#)]
27. Pan, L.; Pei, X.; He, R.; Wan, Q.; Wang, J. Multiwall carbon nanotubes/polycaprolactone composites for bone tissue engineering application. *Colloids Surf. B Biointerfaces* **2012**, *93*, 226–234. [[CrossRef](#)] [[PubMed](#)]
28. Islam, M.; Masum, S.; Rahman, M.M.; Islam, A.; Shaikh, A.A. Preparation of Chitosan from Shrimp Shell and Investigation of Its Properties. *Int. J. Basic Appl. Sci.* **2011**, *11*, 77–80.
29. Pinto, L.C.M. *Quantikov Um Analisador Microestrutural Para o Ambiente Windows*; Instituto de Pesquisas Energéticas e Nucleares: São Paulo, Brazil, 1996.
30. Liberman, A.; Mendez, N.; Trogler, W.C.; Kummel, A.C. Synthesis and surface functionalization of silica nanoparticles for nanomedicine. *Surf. Sci. Rep.* **2014**, *69*, 132–158. [[CrossRef](#)] [[PubMed](#)]
31. Hu, X.; Wang, Y.; Peng, B. Chitosan-capped mesoporous silica nanoparticles as pH-responsive nanocarriers for controlled drug release. *Chem. Asian J.* **2013**, *9*, 319–327. [[CrossRef](#)] [[PubMed](#)]
32. Kim, T.H.; Kim, M.; Eltohamy, M.; Yun, Y.R.; Jang, J.H.; Kim, H.W. Efficacy of mesoporous silica nanoparticles in delivering BMP-2 plasmid DNA for in vitro osteogenic stimulation of mesenchymal stem cells. *J. Biomed. Mater. Res. Part A* **2013**, *101*, 1651–1660. [[CrossRef](#)] [[PubMed](#)]
33. Tao, C.; Zhu, Y.; Xu, Y.; Zhu, M.; Morita, H.; Hanagata, N. Mesoporous silica nanoparticles for enhancing the delivery efficiency of immunostimulatory DNA drugs. *Dalton Trans.* **2014**, *43*, 5142–5150. [[CrossRef](#)] [[PubMed](#)]
34. Zhang, Y.; Wang, Z.; Zhou, W.; Min, G.; Lang, M. Cationic poly(ϵ -caprolactone) surface functionalized mesoporous silica nanoparticles and their application in drug delivery. *Appl. Surf. Sci.* **2013**, *276*, 769–775. [[CrossRef](#)]
35. Xia, T.; Kovoichich, M.; Liang, M.; Meng, H.; Kabehie, S.; George, S.; Zink, J.I.; Nel, A.E. Polyethyleneimine coating enhances the cellular uptake of mesoporous silica nanoparticles and allows safe delivery of sirna and dna constructs. *ACS Nano* **2009**, *3*, 3273–3286. [[CrossRef](#)] [[PubMed](#)]
36. Zhang, S.; Xu, Y.; Wang, B.; Qiao, W.; Liu, D. Cationic compounds used in lipoplexes and polyplexes for gene delivery. *J. Control. Release* **2004**, *100*, 165–180. [[CrossRef](#)] [[PubMed](#)]
37. Deng, Z.; Zhen, Z.; Hu, X.; Wu, S.; Xu, Z.; Chu, P.K. Hollow chitosan-silica nanospheres as pH-sensitive targeted delivery carriers in breast cancer therapy. *Biomaterials* **2011**, *32*, 4976–4986. [[CrossRef](#)] [[PubMed](#)]
38. Lee, K.; Kwon, I.; Kim, Y.-H.; Jo, W.; Jeong, S. Preparation of chitosan self-aggregates as a gene delivery system. *J. Control. Release* **1998**, *51*, 213–220. [[CrossRef](#)]

